

www.acsami.org Research Article

One-Dimensional, Titania Lepidocrocite-Based Nanofilaments and Their Polysulfide Anchoring Capabilities in Lithium—Sulfur Batteries

Neal A. Cardoza, Hussein O. Badr, Rhyz Pereira, Michel W. Barsoum, and Vibha Kalra*



Cite This: ACS Appl. Mater. Interfaces 2023, 15, 50973–50980



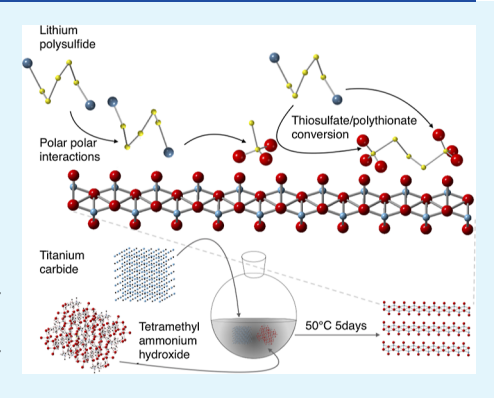
ACCESS I

Metrics & More

Article Recommendations

Supporting Information

ABSTRACT: The high theoretical energy density of metal—sulfur batteries compared to their lithium-ion counter parts renders sulfur-based electrode chemistries attractive. Additionally, sulfur is relatively abundant and environmentally benign. Yet, issues like the low conductivity of sulfur, polysulfide (PS) formation, and shuttling have hindered the development of sulfur chemistries. Here, we react titanium carbide powders with tetramethylammonium hydroxide ammonium salts at 50 °C for 5 days and convert them into one dimensional, titania-based lepidocrocite (1DL) nanofilaments (NFs) using our facile bottom-up approach. This simple and scalable approach led to better electrode functionalization, facile tunability, and a higher density of active sites. The 1DL NFs self-assembled into a variety of microstructures—from individual 1DL NFs with minimal cross sections $\approx 5 \times 7 ~\rm Å^2$ to 2D flakes to mesoscopic particles. A composite was made with a 1:1 weight ratio of sulfur and 1DL NFs, which were hand-ground, mixed with carbon black and binder in



a weight ratio of 70:20:10, respectively. We obtained a specific capacity of 750 mA h g⁻¹ at 0.5C for 300 cycles. The 1DL NFs that, in this case assembled into 2D layers, trapped the polysulfides, PSs, by forming thiosulfate species and Lewis acid—base interactions with the Ti, as confirmed by post-mortem X-ray photoelectron spectroscopy. These interactions were also confirmed by PS adsorption via UV—vis spectroscopy and shuttle current measurements that showed lower PS shuttling in the 1DL NFs cells.

KEYWORDS: Li-S batteries, energy storage, scalable one-dimensional (1D) nanofilaments, lepidocrocite titania-based nanostructures, bottom-up synthesis

■ INTRODUCTION

As the world looks toward renewable energies to decarbonize, their intermittent nature demands better batteries. ^{1,2} The reliability and maturity of lithium ion batteries, LIB, have allowed them to dominate the current commercial market. ^{3–5} This dominance extends to the current electric vehicle market. To improve the adoption of electric vehicles, newer chemistries, with larger specific capacities, are sought after in order to increase the driving range. ^{6–8} At \approx 274 mA h g⁻¹, the practical specific capacities of LIB are relatively low. Additionally, lithium-ion cathodes employ expensive and toxic elements.

Elemental sulfur (S) is one of the highest specific capacity cathode materials that are soluble in the electrolyte and result in the notorious P (1672 mA h g⁻¹), second only to oxygen.⁹ Additionally S is cheap and nontoxic.¹⁰ These reasons, among others, render the lithium–sulfur (Li–S) chemistry attractive for next-generation energy storage devices. However, even after decades of development, its commercial potential is yet to be recognized.¹¹ Issues that plague its development include high-capacity fade, poor cycle life, and low S utilization. These still need to be addressed.^{12,13} These issues can be largely attributed to the polysulfide (PS) shuttle and the insulating nature of S. The reduction of S to lithium sulfides forms PSs.

These PSs (Li_2S_x , 2 < x < 8) are soluble in the electrolyte and result in the notorious PS shuttle effect. These PSs also reduce on the Li anode, forming a passivating film of lithium sulfide (Li_2S) which, in turn, contributes to active material loss. In recent years, various approaches have been taken to mitigate the PS shuttle effect. These include the use of carbon (C) host materials, electrocatalysts, and redox mediators, among others. $^{13,15-17}$

One popular approach is to use a C host material to primarily increase the conductivity of the S-cathode and possibly to confine S in C pores or in 2D nanostructures. For example, Dai et al. have shown that S nanospheres wrapped with graphene through electrostatic interactions show improved conductivity and PS deposition through the surface area of the graphene. ¹⁸ Kuang et al. used nitrogen- and borondoped graphene nanoribbons to enhance both the PS adsorption and conductivity. ¹⁹ Recently, Zhang et al. showed

Received: April 23, 2023 Accepted: August 17, 2023 Published: October 27, 2023





that TiC grafted onto graphene upon nanofiber heterostructures via electrospinning can yield improved electrocatalytic properties. However, most of these approaches have the drawback of synthesis complexity.²⁰

MXenes are another class of 2D nanomaterials that have excelled as host materials for sulfur. In the past, we used di(hydrogenated tallow)benzylmethylammonium chloride to functionalize the surface of MXenes and to enhance their contact with S. 21,22 This functionalized MXenes through a carbon disulfide solvent deposition enables higher utilization and faster kinetics of the PS reactions.²² Additionally, vapor deposition of S on the functionalized MXenes enable the use of carbonate electrolytes.²³ MXenes are also great sulfur hosts without modification due to their surface functionalities and high electronic conductivities.²⁴ However, the drawbacks to using MXenes are primarily their synthesis complexity, inherent instability toward oxidation, and relatively high cost.

Recently, we discovered a process to make one-dimensional (1D) lepidocrocite-based nanofilaments (NFs), henceforth termed 1DL NFs. The method is solution-precipitation-based, one pot, inexpensive, bottom-up, and highly scalable. Interestingly, depending on how they are washed, these 1DL NFs self-assemble into a large variety of structures, from 2D flakes to mesoscopic particles to fiber bundles. 25,26 To manufacture our materials, we immersed water insoluble Ticontaining precursors—such as TiC, TiB2, TiN, TiSi2, etc.—in 25 wt % tetramethylammonium hydroxide (TMAH) aqueous solution in the 50-80 °C temperature range in plastic bottles, under ambient pressure, for a few days and transformed them into 1DL NFs.²⁷ The cross sections of the NFs are $\approx 5 \times 7 \text{ Å}^2$, viz., and they are truly 1D in that quantum size effects come into play.²⁸ They are also exceedingly stable in water (>6 month) even when irradiated with a Xe lamp while stirring.²

Herein, we demonstrate how TiC-derived 1DL NFs formed at 50 or 80 °C can be used as PS anchors. Cathodes made by simple mechanical mixing of the 1DL NFs and S-without melting or vaporizing—still yielded capacities of \approx 750 mA h g⁻¹ after 300 cycles at a rate of 0.5C. This stability is enabled by the polar-polar interactions of PSs with the surface hydroxide groups and Lewis acid-base interactions with the 1DL NFs.

EXPERIMENTAL METHODS

Preparation of TiC-Derived 1DL NFs. The 1DL NFs were prepared as described in our previous paper.²⁷ Briefly, commercial ~200 mesh titanium carbide, TiC, (purity, 99+% metal basis, Alfa Aesar, USA) powders were immersed in a 25 wt % TMAH aqueous solution (Alfa Aesar, 99.9999%) in a ratio of 1 g to 10 mL of TMAH solution. The mixture was then reacted at 50 °C for 5 days or at 80 °C for 3 days with vigorous stirring on a magnetic stir plate. The obtained product was then washed with absolute ethanol (Decon Lab, 200 proof, PA) by centrifugation, and the supernatant was discarded, while the pellet was kept. The washing process was repeated five times until a neutral pH is reached. Centrifugation was carried out at 3500 rpm for 5 min in a centrifuge (Beckman Allegra 64R, USA)

The 1DL NFs were extracted by mixing the resulting pellet from the ethanol wash with DI water to form a colloidal suspension and centrifuging it at 3500 rpm for 30 min. During the DI water wash, the supernatant was kept, and the sediment consisting of mainly unreacted TiC was discarded after second DI water wash. The colloid was then mixed with 5 M lithium chloride, LiCl, (anhydrous 99%, -20 mesh, Alfa Aesar, USA) at a ratio of 2 times by volume of the colloidal suspension and stirred for 24 h. The resultant mixture was then washed with DI water and centrifuged to remove any LiCl leftover salt. The resulting suspension was then sonicated with argon,

Ar, (Airgas, USA) bubbling at a temperature held below 15 °C for 2 h. Lastly, the suspension was vacuum filtered and freeze-dried to form powders comprising 1DL NFs.

Preparation of Electrodes for Li-S Cells. The composite electrodes were made by using a typical slurry method. For example, for a 100 mg slurry, 35 mg of freeze-dried TiC-based 1DL NFs was combined with 35 mg of S (sublimed, 100 mesh, 99.5%, Alfa Aesar, USA) to form the S/1DL NFs composite. Then, 20 mg of conductive carbon Super P (conductive, 99+% metal basis, Alfa Aesar, USA) was added with 10 mg of battery-grade polyvinylidene fluoride (PVDF) binder (MTI, China). The powders were combined by dropwise addition of 400 µL N-methyl-2-pyrrolidone (NMP; TCI, Japan), and typically about four zirconia grinding balls were added (two 2.5 mm balls and two 5 mm balls Uxcell, China). The slurry was then mixed for 8 min in total at 2000 rpm in a planetary FlackTek SpeedMixer, at which point the slurry reached the desired consistency. The resultant slurry was blade-cast on an aluminum (Al) foil (Fisher Scientific, USA). After being cast, the foil was dried in a vacuum oven at 50 °C for 12 h and retrieved once it had cooled back to room temperature, RT. The last step was to freeze-dry the electrodes under liquid nitrogen (Airgas, USA) held under vacuum for 24 h, with the first hour being at 50 °C in a vacuum oven. This step was used to remove any last vestiges of water from the electrode.

Coin Cell Fabrication. The dried Al sheet coated with 1DL NFs was punched into 11 mm diameter cathodes for use in coin cells. These were then weighed and transferred to the antechamber of an Ar-filled (Airgas, USA) glovebox (Mbraun, Germany, LABstar, O2 < 1 ppm and H₂O < 1 ppm). The electrodes were assembled into CR2032 (MTI and Xiamen TMAX Battery Equipment, China) cointype cells. The assembly also included 13 mm diameter disks of 750 µm thick lithium metal foil (Alfa Aesar, USA) and a 19 mm Celgard 2325 separator. The Li metal foil was placed on a stainless-steel spacer, and pressure was provided by a stainless-steel spring.

The electrolyte used was 1 M lithium bis-(trifluoromethanesulfonyl)imide (LiTFSi) with 1 wt % lithium nitrate (LiNO₃) in a mixture of 1,2-dimethoxyethane and 1,3-dioxolane at a 1:1 volume ratio. The electrolyte (Gotion, USA) had a water content of <1 ppm. The amount of electrolyte was fixed with the electrolyte to S ratio of 20 μ L mg⁻¹. The coin cells were then crimped and rested for 10 h. The open-circuit voltage, OCV, was on average 2.3 V.

Galvanostatic tests were conducted on a multichannel cycler (MACCOR 4000 series, USA) and a battery cycler (Neware BTS 4000, China). Cyclic stability tests were performed at RT in the voltage range of 1.8-2.6 V vs Li/Li⁺ after two cycles at 0.1 C and two cycles at 0.2 C as conditioning cycles (1 C = 1672 mA h g^{-1}). Cyclic voltammetry was performed using a potentiostat (VMP3, Biologic, France) in the voltage range of 1.8 to 2.6 V vs Li/Li⁺ at scan rates ranging from 0.1 to 0.5 mV s⁻¹. Electrochemical impedance spectroscopy was performed on the same potentiostat over the 10 mHz to 1 MHz frequency regime. A shuttle current test was also performed on the same potentiostat using methods described in the literature.³⁰ Briefly, the cells were cycled in the galvanostatic mode three times at 0.05 C as formation cycling, and then the cells were allowed to relax back to the OCV for 10 s. Following that, chronoamperometry was performed for 2 h by holding the voltage of the cell at the OCV. The changes in the current during this stage are measures of the PS shuttling current.

Material Characterization. X-ray diffraction (XRD) was used to characterize the 1DL NFs on a powder diffractometer (MiniFlex, Rigaku, Japan) using Cu K α radiation (40 kV and 15 mA), with a step size of 0.02 in the 5 to 60° 2θ range. X-ray photoelectron spectroscopy (XPS) was performed on a spectrometer (Physical Electronics VersaProbe 5000) with an Al K α source with 1486.2 eV. An Ar milling gun was used for the post-mortem cycled cathodes to remove the electrolyte and other surface species.

A scanning electron microscope, SEM (Zeiss Supra VP50), with field emission scanning, was used to characterize the morphology of our materials and devices. The SEM is equipped with an Everhart-Thornley secondary electron detector and an energy-dispersive spectrometer (Oxford Ultim Max 40 mm, UK) with a silicon drift

detector for elemental analysis. The S weight percent in the composite slurry was determined using a thermogravimetric analyzer, TGA (Setaram Setline STA), in ultrahigh purity nitrogen (Airgas) heated at 5 °C min⁻¹ with a flow rate of 0.15 L min⁻¹.

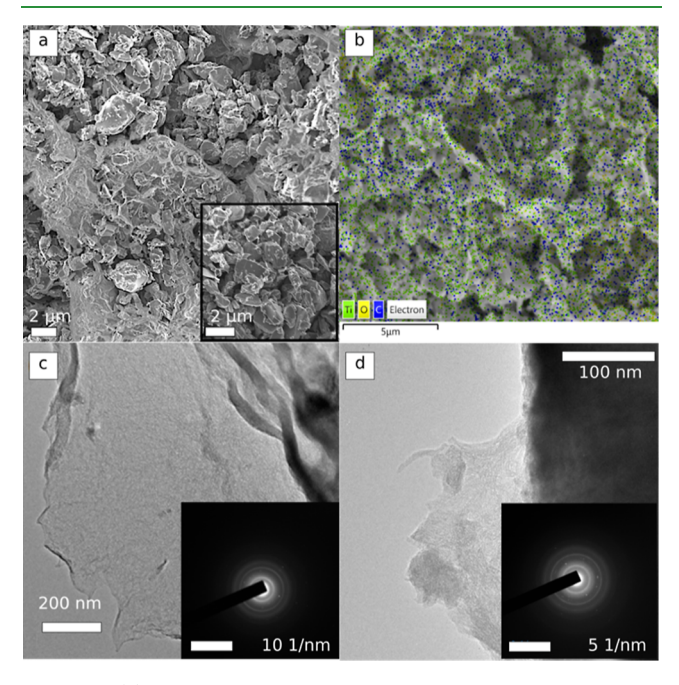


Figure 1. (a) SEM image of 50 °C 5 d TiC-derived 1DL NFs. Inset shows a higher-magnification image of 1DL NFs. (b) EDS map of 50 °C 5 d TiC-derived 1DL NFs, showing the presence of Ti, O, and C. TEM images of (c) TiC-derived sample (50 °C for 5d) showing 1DL NFs assembled in 2D sheets. (d) Similar to (c) but for TiC powders reacted at 80 °C for 3d. Insets in (c, d) show the corresponding SAD patterns for the NFs/2D sheets shown in the panels. Morphological changes are further explored in Badr et al., 2023. 31

Additionally, a field emission transmission electron microscope, TEM (JEOL 2100F, Japan), was used to image the materials used. The 1DL NFs powders were crushed and dispersed in isopropyl alcohol on a TEM grid. UV–vis spectroscopy was conducted on a spectrophotometer (Cary 60 UV–vis Agilent, USA) with a Xenon flash lamp (80 Hz) at a scan speed of 300 nm min⁻¹.

Lithium PS Solution. First, a solution was made by mixing S and Li_2S in stoichiometric proportions to create a 10 mM Li_2S_6 solution

with equal parts of 1,3-dioxolane (DOL) and 1,2-dimethoxyethane (DME). The solution of S, Li₂S, DOL, and DME was stirred overnight at 40 $^{\circ}$ C in a glovebox under Ar. The now cooled stock solution was then diluted to 2 and 0.5 mM and then used as is.

■ RESULTS AND DISCUSSION

Effect of TiC-Based 1DL NFs on the Performance of Li-S Batteries. The 1DL NFs with their nanosheet-like structure made from NFs with a functionalized surface and a high surface area can be used as a S host material. The morphology and structure were determined by SEM energydispersive X-ray spectrometry (EDS), and TEM can be seen in Figure 1. Additional XRD patterns can be seen in Figure S1. In the XRD signature, a set of three intense diffraction peaks were observed that correspond to unreacted crystalline precursor TiC. For the 1DL NFs, a broad peak located at $\sim 9^{\circ} 2\theta$ value is ascribed to the (010) basal plane of the Li⁺ ions-intercalated 1DL NFs. Additionally, we noticed minor broad peaks at $\sim 27^{\circ}$ 2θ and $\sim 48^{\circ}$ 2θ that are consistent with the 110 and 200 reflections of the lepidocrocite titania structure. Turning to the nanofilaments' composition, EDS confirms the presence of Ti, O, and C elements in the 1DL NFs. SEM shows nanoflakes that have agglomerated, and TEM images show that these nanoflakes are made up of nanofilaments. The selected area diffraction (SAD) patterns of the 1DL NF-based sheets (insets in Figure 1c,d) clearly demostrate two arcs, which correspond to the two XRD reflections observed round $\sim 25^{\circ}$ and $\sim 48^{\circ}$ 2θ values (Figure S1).

In evaluating the effectiveness of our 1DL NFs as cathodes in Li–S batteries, we assembled coin cells with a loading of 1 mg cm $^{-2}$, in which 35 wt. % is S, as determined by TGA (Figure S3). Typical S voltage plateaus are observed in Figure 2. The 1DL NFs also show stable long-term cycling, as seen in Figure 2. When the cell was cycled at 0.5C, a capacity of \approx 750 mA h g $^{-1}$ was retained for 300 cycles after which it faded. Additionally, the 1DL NF-based electrodes show good rate capability, as seen in Figure 3.

The fade in the capacity (Figure 3a) can be attributed to a few factors. First, there could be a decrease in PS retention over the course of cycling. The available active sites on the 1DL NFs could also decrease over the course of cycling. This can be seen in the shrinkage of the lower reduction plateau at 2.1 V, which is largely where soluble PSs reduce to insoluble

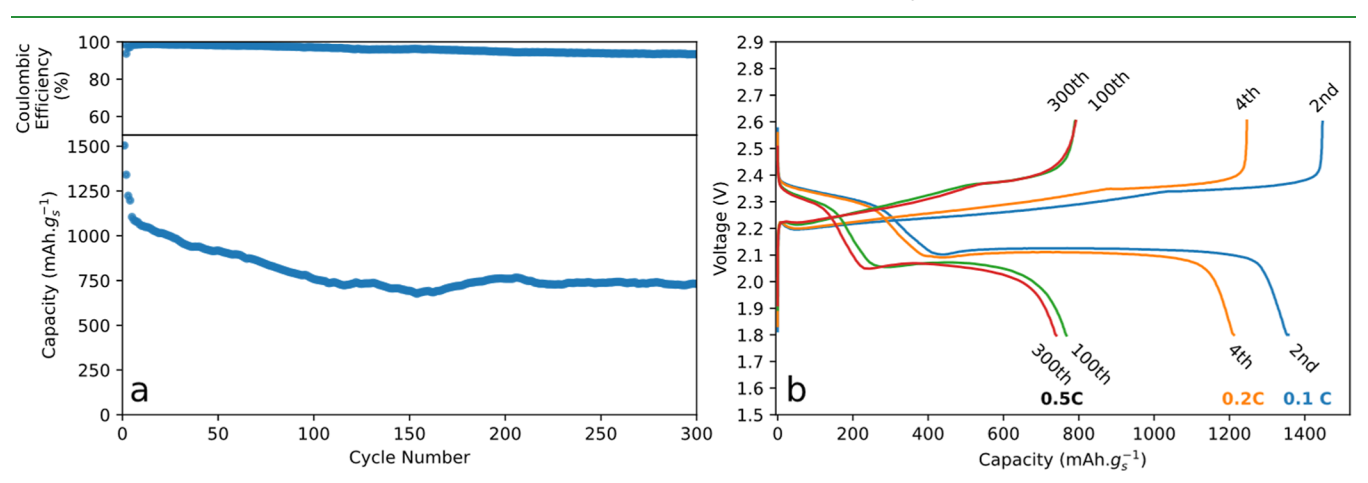


Figure 2. Electrochemical cycling of TiC-derived 1DL NFs S composites, making up 70 wt % of the cathode with 35 wt % sulfur, with an areal loading of 1 mg cm $^{-2}$. Flake-like structure of the 50 °C 1DL NFs shows a higher initial capacity with rapid initial fading, attributed to the volumetric expansion of S microcracking the microstructure. (a) Specific capacity vs cycles and (b) voltage profile plot.

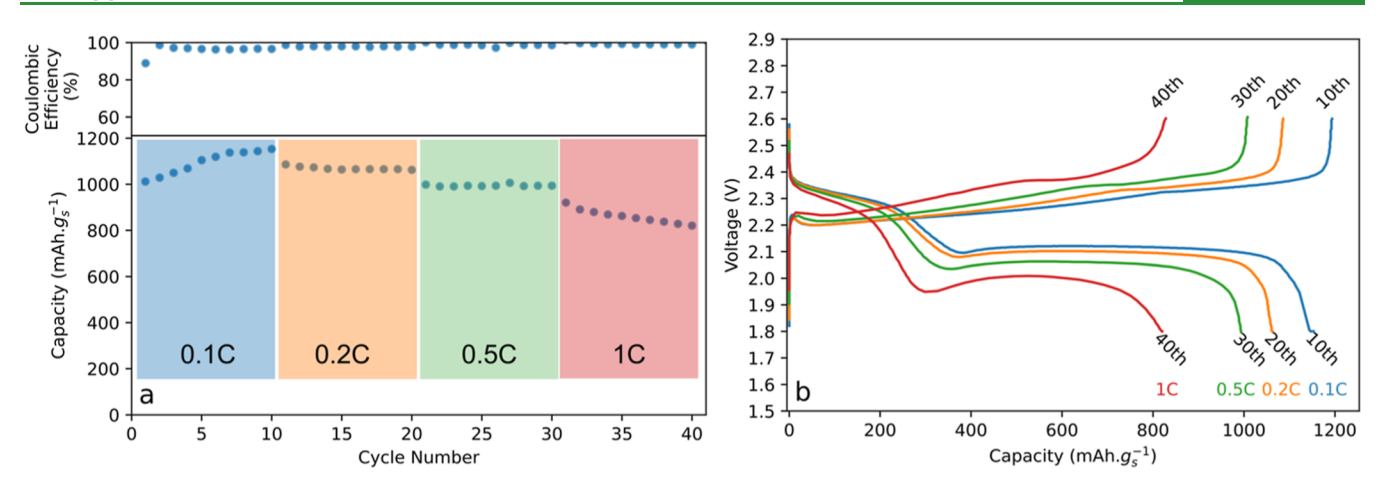


Figure 3. Rate study of 50 °C 5d TiC-derived 1DL NFS with 35 wt % S for a loading of 0.74 mg cm⁻², demonstrating good rate capability at 1C. (a) Specific capacity over C-rates of 0.1–1C and (b) voltage profiles for respective C-rates.

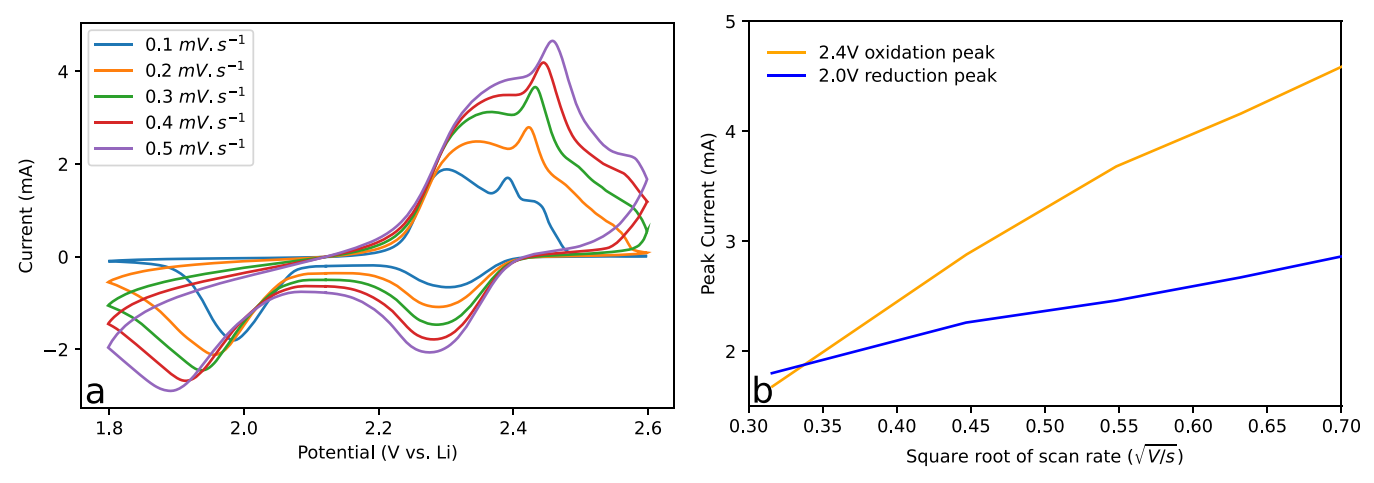


Figure 4. (a) CV of TiC-derived 1DL NFs synthesized at 50 $^{\circ}$ C for 5 days with 35 wt % S and a loading of 0.74 mg cm⁻². (b) Randles–Sevcik plot of the 2.4 and 2.0 V peaks at scan rates from 0.1 to 0.5 mV s⁻¹.

PSs. However, the shrinkage of the upper reduction plateau at 2.3 V is indicative of a loss of S. The loss can also be seen as a decrease in Coulombic efficiency prefacing the decrease in specific capacity. This leads to a second factor, which is the loss of electrochemically active Li₂S to inaccessible locations on both the cathode and the anode. Additionally, over the course of cycling, there is an increase in polarization that can be attributed to an increase in the passivating nature of the Li₂S.

To ensure that the increase in capacity is not from the 1DL NFs acting as an active material, a cell test was constructed, wherein an electrode consisting of 90% TiC-derived 1DL NFs and 10% PVDF was cast and dried under the same conditions as for the S-containing electrodes. After weighing, it was assembled into a CR2032 cell with 20 μ L of electrolyte. This cell was cycled, with an arbitrarily low constant current of 0.24 μ A from 2.6 to 1.8 V. Upon approaching 1.8 V, it was held at that voltage until the current dropped to below 0.01 μ A. This was then repeated. The results Figure S4 were clear: the capacity of the first cycle was 5 mA h g⁻¹, while that of the second was 1.4 mA h g⁻¹. We can thus conclude that the additional capacity achieved in the Li–S cathodes is due to the presence of S.

Figure 4 shows the cyclic voltammetry (CV) curves of the 1DL NFs-S composites in cells at various scan rates to probe the redox reactions. Two reduction peaks are observed at all

scan rates. The reduction peak at 2.3 V corresponds to the higher order PS conversion (Li_2S_8 to Li_2S_5). The reduction peak at 2.0 V, on the other hand, corresponds to Li_2S_4 and Li_2S_2 reducing to Li_2S . Increasing the scan rate shows higher peak separation of the lower redox peaks. This indicates that while 1DL NFs exhibit PS adsorption, as seen in Figures 5 and 6 with UV—vis and shuttle current measurements, they do not improve the kinetics of the soluble to insoluble PS conversion.

Mechanism of TiC-Based 1DL NFs—PS Retention. To initially probe the existence of an interaction between our 1DL NFs and PSs, a visual absorption test was conducted. For comparison purposes, the test was repeated with C black. To carry out the test, 1DL NFs or C black was added to vials containing the PS solutions, and a picture was taken initially and after a week. The results (Figures 5 and S5) show that after 7 d, the solution in the vial containing 0.5 mM concentration of PS and 1DL was clear. In contrast, the solution with C-black remained colored. At higher PS concentrations, the results are the same except that not all of the PSs are adsorbed on the 1DL NFs.

To quantify these observations, the solutions were analyzed on a UV–vis spectrophotometer. Here again, the results are quite clear: after 7 d in the vial containing the 1DL NFs, the peak at 360 nm (attributed to $\rm S_6^{2-}$ in the DOL and DME solution $\rm ^{32}$) is absent. That peak, however, is present in the vial

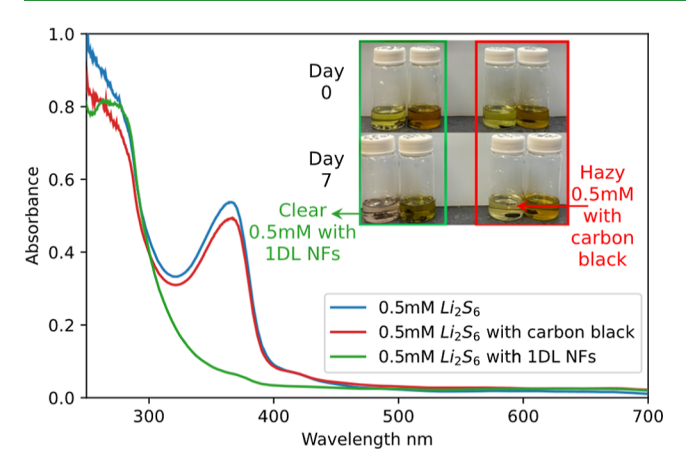


Figure 5. UV-vis spectrum showing the effectiveness of 1DL NFs in adsorbing PSs. Inset shows pictures of different vials used to observe interactions with TiC 1DL NFs. Compared to C black, the 1DL NFs can remove more PSs as seen in the picture after 7 days, indicating that C black does not cause a significant amount of PS adsorption relative to TiC 1DL NFs, when combined in the electrode. Larger image is given in the Supporting Information.

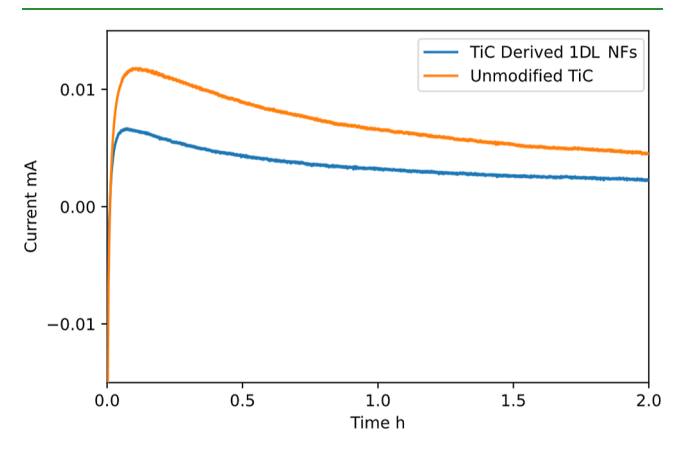


Figure 6. Shuttle current experiment showing enhanced PS adsorbing ability of TiC-derived 1DL NFs in comparison to unmodified TiC. This figure demonstrates that the conversion of TiC to the 1DL NFs structure enables the adsorption of PS.

containing only black C black. This is a clear indication that the TiC-derived 1DL NFs adsorb more PSs than C black.

A shuttle current was used to probe the level of PSs in the cell. As PSs that shuttle cause self-discharge, holding a cell at a voltage where PSs are known to be active would need a higher current to counteract the self-discharging of the PS. Hence, a higher current can be correlated to a higher concentration of PSs. The results can be seen in Figure 6, which is the recorded current for 2h at a potentiostatic hold at OCV.

XPS high-resolution spectra of cycled 1DL NFs cathode surfaces in the Ti 2p, S 2p, and C 1s regions are shown in Figure 7d-f, respectively. The corresponding spectra for the pristine cathodes before cycling are shown in Figure 7a-c. The cycled cathode was extracted, in an Ar-filled glovebox, from a cell that was cycled at 0.1 mV s⁻¹ for 5 cycles between 1.8 and 2.6 V and then held at 2.1 V for 3 h until it was transferred into the glovebox. An air-tight transfer chamber was used to move the cathode to the XPS chamber without it being exposed to the atmosphere. Ar milling for a total of 20 min, consisting of two runs each of 10 min was used to remove any residual electrolyte products from the cathode's surface. This revealed a

multitude of peaks for the S 2p spectrum (Figure 7e) that were not present in the pristine samples (Figure 7b). One of the peaks with a binding energy, BE, of 164 eV can be attributed to the central S in PSs, likely occurring due to an incomplete conversion.³³ Additionally, the peak at 159.9 eV is attributed to Li₂S as a discharge product.^{33,34} This probe revealed that there were two types of interactions between the S and the 1DL

The first interaction appears to be due to the formation of thiosulfate and polythionate groups. Peaks at BEs of 167.1 and 168.3 eV (Figure 7e) can be attributed to polythionate and thiosulfate species, respectively. 35-37 This is like other metal oxides that function as electrocatalysts.35 This interaction is similar to the one proposed for PS anchoring of MXenes, 37,38 where the hydroxyl groups on the surface are consumed by the PS to form thiosulfate/polythionate compounds. These compounds, in turn, trap the PSs but are still electrochemically active. As these hydroxyl surface groups are consumed on the 1DL NFs, more Ti atoms are exposed to the PSs leading to Lewis acid—base interactions.

Lewis acid-base interactions are the second mechanism of PS trapping by the 1DL NFs. This can best be seen when the pristine TiC 1DL NFs XPS results are compared to those of TiO₂ (Figure 7a). In the pristine sample (Figure 7a), we see two peaks at BEs of 458.9 and 464.6 eV that can be attributed to TiO.³⁹⁻⁴¹ The post-mortem Ti 2p two peaks also appear, although their shapes and positions are vastly different than the pristine sample. These two peaks are a combination of several peaks. One of them is the Ti-S peak at 456.5 and 462.2 eV in addition to the 1DL NFs TiO peaks, and unreacted TiC peaks are observed.

The Ti-S peaks were not observed in the pristine electrodes, which confirms that it is only after electrochemical cycling that these peaks appear. 22,42 Consistently, this interaction also manifests itself in the S 2p spectrum (Figure 7e) as peaks with BEs of 161.6 eV and 162.8.^{22,42} The Lewis acid-base interaction can be summarized as a vacant orbital on the Ti atoms and a filled orbital on the PSs. Here, the Ti atoms act as a Lewis acid, and the PSs act as the Lewis base. Additionally, upon comparing the Ti-O peaks from the pristine and the post-mortem in the Ti 2p spectrum, we notice a shift in the BEs. This shift could be attributed to the change in the coordination number of Ti atoms, further lending credence to the Lewis acid-base-type interactions between the PSs and the 1DL NFs.

CONCLUSIONS

A radically new bottom-up approach that is both facile and scalable and uses earth-abundant materials was used to make 1DL NFs of which some self-assembled into nanosheets. The obtained material not only served as an S-host material but also appeared to anchor PSs. Based on XPS data, we believe there are two mechanisms of PS anchoring; the first is the polarpolar interactions with a hydroxide-functionalized surface and the second is the Lewis acid-base interactions with titanium, resulting in Ti-S bonds. It is through these interactions that cathodes made by simple mechanical mixing, that is, without melting or vaporizing the S into the TiC-based NFs, can store 750 mA h g⁻¹ after 300 cycles at 0.5C. The 1DL NFs can come in a range of nanostructures from flakes to nanowires. This opens up an exciting range of possibilities for new S 2D-host nanostructures with surface functionalization.

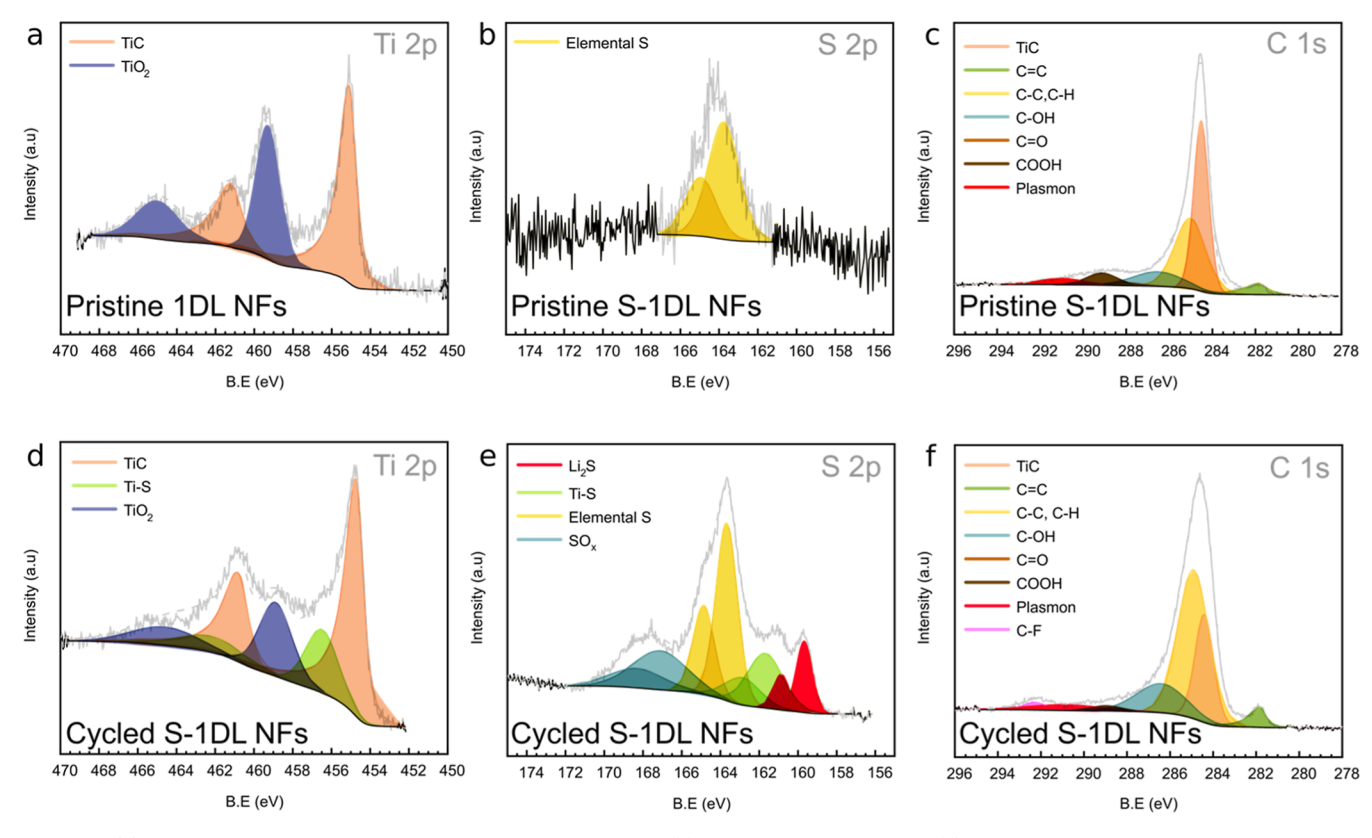


Figure 7. (a) XPS spectrum of pristine TiC-derived 1DL NFs, Ti 2p, (b) XPS S 2p spectrum, and (c) XPS C 1s spectrum of pristine S-1DL NFs cathode as fabricated. (d-f) Ti 2p, S 2p, and C 1s spectra are post-mortem cathode after argon sputtering. Post-mortem spectra show the formation of the thionate/polythionate groups and Ti–S. Leading to the two mechanism of PS binding, electrocatalyst and Lewis acid—base interactions.

ASSOCIATED CONTENT

Supporting Information

The Supporting Information is available free of charge at https://pubs.acs.org/doi/10.1021/acsami.3c03743.

Additional material characterization of 1DL NFs, additional electrochemical tests of 1DL NFs and TiC control, post-mortem SEM images of the cathode, and TGA curves of the as-used cathode in electrochemical tests (PDF)

AUTHOR INFORMATION

Corresponding Author

Vibha Kalra — Department of Chemical and Biological Engineering, Drexel University, Philadelphia PA-19104, Pennsylvania; orcid.org/0000-0002-2630-1560; Email: vk99@drexel.edu

Authors

Neal A. Cardoza – Department of Chemical and Biological Engineering, Drexel University, Philadelphia PA-19104, Pennsylvania

Hussein O. Badr – Department of Material Science Engineering, Drexel University, Philadelphia PA-19104, Pennsylvania

Rhyz Pereira — Department of Chemical and Biological Engineering, Drexel University, Philadelphia PA-19104, Pennsylvania

Michel W. Barsoum — Department of Material Science Engineering, Drexel University, Philadelphia PA-19104, Pennsylvania; Oorcid.org/0000-0001-7800-3517 Complete contact information is available at: https://pubs.acs.org/10.1021/acsami.3c03743

Author Contributions

The manuscript was written through contributions of all authors. All authors have given approval to the final version of the manuscript.

Funding

This work was supported by the National Science Foundation grants 2211049 and 1919177.

Notes

The authors declare no competing financial interest.

ACKNOWLEDGMENTS

We thank the National Science Foundation for their support. We are grateful for the help and usage of the instruments at the Drexel Material Characterization Center RRID:SCR_022684. We thank Professor Barsoum's group for providing material insight and guidance for the synthesis of 1DL NFs. The authors also would like to thank Dr. V. Natu for helping in the XPS analysis and discussion.

ABBREVIATIONS

1DL NFs	one-dimensional	lepidocrocite	titania-
	based nanofilame	ents	
2D	two-dimensional		
S	sulfur		
Li-S	lithium-sulfur		
PSs	polysulfides		
Li	lithium		

 $\begin{array}{ccc} \text{Li}_2S & & \text{lithium sulfide} \\ \text{C} & & \text{carbon} \\ \text{Ar} & & \text{argon} \end{array}$

TMAH tetramethylammonium hydroxide

 $\begin{array}{ll} TiC & titanium \ carbide \\ TiO_2 & titanium \ oxide \\ TiN & titanium \ nitride \\ TiB_2 & titanium \ boride \\ \end{array}$

LiTFSi lithium bis(trifluoromethanesulfonyl)-

imide

LiNO₃ lithium nitrate
DME 1,2-dimethoxyethane
DOL 1,3-dioxolane
OCV open-circuit voltage

XPS X-ray photoelectron spectroscopy
SEM scanning electron microscopy
TEM transmissions electron microscopy

SAD selected area diffraction

EDS energy dispersive X-ray spectrometry

TGA thermogravimetric analysis UV-vis spectrometer ultraviolet-visible spectrometer

REFERENCES

- (1) Arbabzadeh, M.; Sioshansi, R.; Johnson, J. X.; Keoleian, G. A. The Role of Energy Storage in Deep Decarbonization of Electricity Production. *Nat. Commun.* **2019**, *10* (1), 3413.
- (2) IEA. Innovation in Batteries and Electricity Storage-A Global Analysis Based on Patent Data, 2020.
- (3) Li, M.; Lu, J.; Chen, Z.; Amine, K. 30 Years of Lithium-Ion Batteries. Adv. Mater. 2018, 30 (33), 1800561.
- (4) Manthiram, A. A Reflection on Lithium-Ion Battery Cathode Chemistry. *Nat. Commun.* **2020**, *11* (1), 1550.
- (5) Xie, J.; Lu, Y.-C. A Retrospective on Lithium-Ion Batteries. *Nat. Commun.* **2020**, *11* (1), 2499.
- (6) Nagai, T. Japanese Policy and NEDO Activity for Future Mobility, New Energy and Industrial Development Organization; NEDO: Japan, 2017. https://www.nedo.go.jp/content/100873093.pdf (accessed June 01, 2022).
- (7) European Council for Automotive R&D (EUCAR). Battery Requirements for Future Automotive Applications; EUCAR, 2019. https://eucar.be/wp-content/uploads/2019/08/20190710-EG-BEV-FCEV-Battery-requirements-FINAL.pdf (accessed June 01, 2022).
- (8) United States Advanced Battery Consortium. USABC Cell Active Material Gap Chart-CY 2025 Commercialization; USABC: Southfield, MI 48075. https://uscar.org/download/246/energy-storage-system-goals/12836/cell-active-material-requirements.pdf (accessed June 01, 2022).
- (9) Kang, W.; Deng, N.; Ju, J.; Li, Q.; Wu, D.; Ma, X.; Li, L.; Naebe, M.; Cheng, B. A Review of Recent Developments in Rechargeable Lithium-Sulfur Batteries. *Nanoscale* **2016**, *8* (37), 16541–16588.
- (10) Manthiram, A.; Chung, S.-H.; Zu, C. Lithium-Sulfur Batteries: Progress and Prospects. *Adv. Mater.* **2015**, 27 (12), 1980–2006.
- (11) Sun, J.; Wang, T.; Gao, Y.; Pan, Z.; Hu, R.; Wang, J. Will lithium-sulfur batteries be the next beyond-lithium ion batteries and even much better? *InfoMat* **2022**, *4* (9), No. e12359, DOI: 10.1002/inf2.12359.
- (12) Urbonaite, S.; Poux, T.; Novák, P. Progress Towards Commercially Viable Li-S Battery Cells. *Adv. Energy Mater.* **2015**, *5* (16), 1500118.
- (13) He, J.; Manthiram, A. A Review on the Status and Challenges of Electrocatalysts in Lithium-Sulfur Batteries. *Energy Storage Mater.* **2019**, *20* (May), 55–70.
- (14) Wang, Z.; Li, Y.; Ji, H.; Zhou, J.; Qian, T.; Yan, C. Unity of Opposites between Soluble and Insoluble Lithium Polysulfides in Lithium-Sulfur Batteries. *Adv. Mater.* **2022**, 34 (47), 2203699.
- (15) Liu, J.; Cao, Y.; Zhou, J.; Wang, M.; Chen, H.; Yang, T.; Sun, Y.; Qian, T.; Yan, C. Artificial Lithium Isopropyl-Sulfide Macro-

- molecules as an Ion-Selective Interface for Long-Life Lithium-Sulfur Batteries. ACS Appl. Mater. Interfaces 2020, 12 (49), 54537-54544.
- (16) Zuo, J.-H.; Zhai, P.-B.; He, Q.-Q.; Wang, L.; Chen, Q.; Gu, X.-K.; Yang, Z.-L.; Gong, Y.-J. In-Situ Constructed Three-Dimensional MoS2-MoN Heterostructure as the Cathode of Lithium-Sulfur Battery. *Rare Met.* **2022**, *41* (5), 1743–1752.
- (17) Li, Z.; Luo, C.; Zhang, S.; Sun, G.; Ma, J.; Wang, X.; He, Y.; Kang, F.; Yang, Q.; Lv, W. Co-recrystallization Induced Self-catalytic Li₂S Cathode Fully Interfaced with Sulfide Catalyst toward a Highperformance Lithium-free Sulfur Battery. *InfoMat* **2022**, 4 (10), No. e12361, DOI: 10.1002/inf2.12361.
- (18) Wang, H.; Yang, Y.; Liang, Y.; Robinson, J. T.; Li, Y.; Jackson, A.; Cui, Y.; Dai, H. Graphene-Wrapped Sulfur Particles as a Rechargeable Lithium-Sulfur Battery Cathode Material with High Capacity and Cycling Stability. *Nano Lett.* **2011**, *11* (7), 2644–2647.
- (19) Chen, L.; Feng, J.; Zhou, H.; Fu, C.; Wang, G.; Yang, L.; Xu, C.; Chen, Z.; Yang, W.; Kuang, Y. Hydrothermal Preparation of Nitrogen, Boron Co-Doped Curved Graphene Nanoribbons with High Dopant Amounts for High-Performance Lithium Sulfur Battery Cathodes. J. Mater. Chem. A 2017, 5 (16), 7403–7415.
- (20) Zhang, Y.; Zhang, P.; Zhang, S.; Wang, Z.; Li, N.; Silva, S. R. P.; Shao, G. A Flexible Metallic TiC Nanofiber/Vertical Graphene 1D/2D Heterostructured as Active Electrocatalyst for Advanced Li-S Batteries. *InfoMat* **2021**, *3* (7), 790–803.
- (21) Carey, M.; Hinton, Z.; Natu, V.; Pai, R.; Sokol, M.; Alvarez, N. J.; Kalra, V.; Barsoum, M. W. Dispersion and Stabilization of Alkylated 2D MXene in Nonpolar Solvents and Their Pseudocapacitive Behavior. *Cell Rep. Phys. Sci.* **2020**, *1* (4), 100042.
- (22) Pai, R.; Natu, V.; Sokol, M.; Carey, M.; Barsoum, M. W.; Kalra, V. Tuning Functional Two-Dimensional MXene Nanosheets to Enable Efficient Sulfur Utilization in Lithium-Sulfur Batteries. *Cell Rep. Phys. Sci.* **2021**, 2 (7), 100480.
- (23) Pai, R.; Natu, V.; Sokol, M.; Carey, M.; Greszler, T.; Barsoum, M. W.; Kalra, V. Sulfur Confined MXene Hosts Enabling the Use of Carbonate-Based Electrolytes in Alkali Metal (Li/Na/K)-Sulfur Batteries. *Mater. Today Energy* **2022**, *27*, 101000.
- (24) Zhu, Q.; Xu, H.-F.; Shen, K.; Zhang, Y.-Z.; Li, B.; Yang, S.-B. Efficient Polysulfides Conversion on Mo2CTx MXene for High-Performance Lithium-Sulfur Batteries. *Rare Met.* **2022**, *41* (1), 311–318.
- (25) Badr, H. O.; Cope, J.; Kono, T.; Torito, T.; Karmakar, A.; Lagunas, F.; Castiel, E.; Klie, R. F.; Barsoum, M. W. Titanium Oxidebased 1D Nanofilaments, 2D Sheets, and Mesoporous Particles: Synthesis, Characterization, and Ion Intercalation. *Matter* **2023**, *6*, 1–17
- (26) Sudhakar, K.; Karmakar, A.; Badr, H. O.; El-Melegy, T.; Hassig, M. Q.; Carey, M.; Masiuk, S.; Wu, L.; Qian, Q.; Kono, T.; Li, C. Y.; Barsoum, M. W. One-dimensional, titania-based lepidocrocite nanofilaments and their self-assembly. *Matter* **2023**, DOI: 10.1016/j.matt.2023.06.006, (in press).
- (27) Badr, H. O.; El-Melegy, T.; Carey, M.; Natu, V.; Hassig, M. Q.; Johnson, C.; Qian, Q.; Li, C. Y.; Kushnir, K.; Colin-Ulloa, E.; Titova, L. V.; Martin, J. L.; Grimm, R. L.; Pai, R.; Kalra, V.; Karmakar, A.; Ruffino, A.; Masiuk, S.; Liang, K.; Naguib, M.; Wilson, O.; Magenau, A.; Montazeri, K.; Zhu, Y.; Cheng, H.; Torita, T.; Koyanagi, M.; Yanagimachi, A.; Ouisse, T.; Barbier, M.; Wilhelm, F.; Rogalev, A.; Björk, J.; Persson, P. O. Å.; Rosen, J.; Hu, Y.-J.; Barsoum, M. W. Bottom-up, Scalable Synthesis of Anatase Nanofilament-Based Two-Dimensional Titanium Carbo-Oxide Flakes. *Mater. Today* 2021, 54, 8.
- (28) Colin-Ulloa, E.; Martin, J. L.; Hanna, R. J.; Frasch, M. H.; Ramthun, R. R.; Badr, H. O.; Uzarski, J. R.; Barsoum, M. W.; Grimm, R. L.; Titova, L. V. Electronic Structure of 1D Lepidocrocite TiO2 as Revealed by Optical Absorption and Photoelectron Spectroscopy. *J. Phys. Chem. C* 2023, 127, 7275–7283.
- (29) Badr, H.; Natu, V.; Neatu, S.; Neau, F.; Kuncser, A.; Rostas, A.; Racey, M.; Barsoum, M. W.; Florea, M. Photo-stable, 1D-nanofilaments ${\rm TiO_2}$ -based lepidocrocite for photocatalytic hydrogen production in water-methanol mixtures. *Matter* **2023**, S2590238523002448.

- (30) Moy, D. Direct Measurement of Polysulfide Shuttle Current: A Window into Understanding the Performance of Lithium-Sulfur Cells. *J. Electrochem. Soc.* **2015**, *162*, A1 DOI: 10.1149/2.0181501jes.
- (31) Badr, H. O.; Lagunas, F.; Autrey, D. E.; Cope, J.; Kono, T.; Torita, T.; Klie, R. F.; Hu, Y.-J.; Barsoum, M. W. On the Structure of One-Dimensional TiO2 Lepidocrocite. *Matter* **2023**, *6* (1), 128–141.
- (32) Zou, Q.; Lu, Y.-C. Solvent-Dictated Lithium Sulfur Redox Reactions: An Operando UV-Vis Spectroscopic Study. *J. Phys. Chem. Lett.* **2016**, 7 (8), 1518–1525.
- (33) Fantauzzi, M.; Elsener, B.; Atzei, D.; Rigoldi, A.; Rossi, A. Exploiting XPS for the Identification of Sulfides and Polysulfides. *RSC Adv.* **2015**, *5* (93), 75953–75963.
- (34) Peng, H. J.; Huang, J. Q.; Cheng, X. B.; Zhang, Q. Review on High-Loading and High-Energy Lithium-Sulfur Batteries. *Adv. Energy Mater.* **2017**, 7 (24), 1700260.
- (35) Liang, X.; Kwok, C. Y.; Lodi-Marzano, F.; Pang, Q.; Cuisinier, M.; Huang, H.; Hart, C. J.; Houtarde, D.; Kaup, K.; Sommer, H.; Brezesinski, T.; Janek, J.; Nazar, L. F. Tuning Transition Metal Oxide-Sulfur Interactions for Long Life Lithium Sulfur Batteries: The "Goldilocks" Principle. *Adv. Energy Mater.* **2016**, 6 (6), 1501636 DOI: 10.1002/aenm.201501636.
- (36) Tang, H.; Li, W.; Pan, L.; Tu, K.; Du, F.; Qiu, T.; Yang, J.; Cullen, C. P.; McEvoy, N.; Zhang, C. (J.). A Robust, Freestanding MXene-Sulfur Conductive Paper for Long-Lifetime Li-S Batteries. *Adv. Funct. Mater.* **2019**, 29 (30), 1901907.
- (37) Tang, H.; Li, W.; Pan, L.; Cullen, C. P.; Liu, Y.; Pakdel, A.; Long, D.; Yang, J.; McEvoy, N.; Duesberg, G. S.; Nicolosi, V.; Zhang, C. J. In Situ Formed Protective Barrier Enabled by Sulfur@Titanium Carbide (MXene) Ink for Achieving High-Capacity, Long Lifetime Li-S Batteries. *Adv. Sci.* **2018**, *5* (9), 1800502.
- (38) Liang, X.; Hart, C.; Pang, Q.; Garsuch, A.; Weiss, T.; Nazar, L. F. A Highly Efficient Polysulfide Mediator for Lithium-Sulfur Batteries. *Nat. Commun.* **2015**, *6* (1), 5682.
- (39) Santerre, F.; El Khakani, M. A.; Chaker, M.; Dodelet, J. P. Properties of TiC Thin Films Grown by Pulsed Laser Deposition. *Appl. Surf. Sci.* **1999**, *148* (1–2), 24–33.
- (40) Diebold, U.; Madey, T. E. TiO ₂ by XPS. Surf. Sci. Spectra **1996**, 4 (3), 227–231.
- (41) Halim, J.; Cook, K. M.; Naguib, M.; Eklund, P.; Gogotsi, Y.; Rosen, J.; Barsoum, M. W. X-Ray Photoelectron Spectroscopy of Select Multi-Layered Transition Metal Carbides (MXenes). *Appl. Surf. Sci.* **2016**, 362, 406–417.
- (42) Franzen, H. F.; Umaña, M. X.; McCreary, J. R.; Thorn, R. J. XPS Spectra of Some Transition Metal and Alkaline Earth Monochalcogenides. *J. Solid State Chem.* **1976**, *18* (4), 363–368.